IEEE Access
Multidisciplinary | Rapid Review | Open Access Journal

Received June 6, 2017, accepted July 3, 2017, date of publication August 29, 2017, date of current version September 27, 2017.

Digital Object Identifier 10.1109/ACCESS.2017.2734699

Sensorless Control of a Shearer Short-Range Cutting Interior Permanent Magnet Synchronous Motor Based on a New Sliding Mode Observer

LIANCHAO SHENG, WEI LI, YUQIAO WANG, MENGBAO FAN, AND XUEFENG YANG
School of Mechatronic Engineering, China University of Mining and Technology, Xuzhou 221116, China

Corresponding author: Wei Li (cmeecumt512@yahoo.com)

This work was supported in part by the National Natural Science Foundation of China under Grant U1610111 and Grant 51307172, in part by the Six Talent Peaks Project in Jiangsu Province under Grant ZBZZ-041, and in part by the Project Funded by the Priority Academic Program Development of the Jiangsu Higher Education Institutions.

ABSTRACT Considering the low reliability and poor adaptability of existing drum shear cutting parts, this paper presents a permanent magnet short-range cutting transmission system with a low-speed and high-torque interior permanent magnet synchronous motor (IPMSM) as the driving source and a sensorless control strategy based on a new sliding mode observer (SMO). To increase the robustness of the observer and reduce the error caused by chattering in the traditional SMO, the phase-locked loop technique is used instead of the traditional arc-tangent function estimation, and the sigmoid function is introduced to replace the traditional sign function; then, the sliding mode gain is adjusted through the fuzzy control algorithm in the new SMO. The scheme effectively improves the problems of the high failure rate caused by the long transmission chain of the shearer cutting section and the environmental impact for the mechanical sensor measurement results. Finally, the mathematical model of IPMSM based on the two-phase rotating coordinate system and end cutting load is established to verify the effectiveness and feasibility of the program. The results show that the new observer can accurately realize the speed and position estimation of the shearer cutting motor, and it has good dynamic response performance, observation accuracy, and robustness.

INDEX TERMS Interior permanent magnet synchronous motor (IPMSM), short-range cutting transmission system, sliding mode observer (SMO), sensorless control.

I. INTRODUCTION

Mining mechanization is a necessary technical method to ensure safe production, production efficiency and improvement of the operating environment in the coal industry, as well as an effective measure for saving manpower, energy and raw materials. A drum shearer is one of the main pieces of equipment for the current fully mechanized coal mining face. Its main cutting transmission mode is "three-phase asynchronous motor + three stage straight gear deceleration + planetary gear reduction + cutting drum." In the cutting process, due to uneven coal seam strength, coal caving brittle rock, hard inclusions and rock interlayers, the load on the drum has the characteristics of randomness, large fluctuation and strong impact [1]–[3], and the shearer cutting rocker has a long transmission chain and multi-drive components, making it a weak part in the shearer. Any gear failure will cause the machine to stop working. According to statistics, planetary gear system failure accounts for 30% of all gear transmission failures [4]. At the same time, previous research on reducing the failure rate of the shearer cutting transmission system consists mainly of the evaluation of its healthy running condition, and the reasons for faults are analyzed. Zhao and Sun [5] and Zhao and Ma [6], [7] used virtual prototyping software to analyze and simulate the vibration characteristics and the reliability of the shearer cutting transmission system and improve the stability of the cutting section through optimizing the transmission system. Si *et al.* [8] employed the vibration of a rocker transmission part and proposed a diagnosis method based on a probabilistic neural network (PNN) and fruit fly optimization algorithm (FOA). Li *et al.* [9] presented a multi-degree of freedom gear model to describe the dynamic behavior of the coal cutter gear systems. The model can be used as a feasible and reliable tool for gear fault mechanism investigation. However, these methods do not substantially reduce the failure probability of the shearer cutting

transmission system, and in the event of failure, maintenance is difficult and the production schedule is affected, which can cause significant economic losses. Therefore, Yang *et al.* [10] proposed a high-reliability short-range cutting transmission system, which can not only effectively shorten the transmission chain and reduce the failure rate but also achieve buffer damping under load mutation and drum speed control under coal seam changes. The inevitable leakage of the hydraulic system and the pipeline elastic deformation will lead to pressure loss and affect the stability of the end drum speed. Therefore, in order to meet the high power, high efficiency, low failure and other performance requirements of the drum shearer, further exploration needs to be done, including driving components, transmission structure, control strategy and other elements. A semi-direct drive system program with a high-power permanent magnet motor [11] can be proposed for reducing the transmission ratio of the shearer cutting transmission system under the existing shearer cutting transmission system installation conditions. The program reduces the transmission parts between the drive motor and the work unit, especially the uselessness of wearing parts such as planetary gears, which can significantly improve system efficiency and reduce failure rates.

Vector control and direct torque control, as well as the variable frequency speed control strategy, are commonly used for mine PMSM. It is necessary to know the position information of the PMSM rotor to achieve closed-loop control. Mechanical sensors such as Hall position sensors and rotary encoders are used in the traditional method. However, the introduction of mechanical sensors not only increases the rotational inertia of the motor shaft and reduces the mechanical properties but also increases the size and volume of PMSM and increases the external hardware line connection, making the system susceptible to interference and instability. Therefore, the sensorless control technology of the IPMSM is particularly important for shearer cutting transmission systems. At the beginning, the IPMSM sensorless control strategy mainly consists of the open-loop estimation method based on the motor mathematical model, such as the mathematical model based on the direct calculation method [12], [13] and the open-loop flux linkage method based on the voltage equation [14]. These methods have the characteristics of simple principles and faster dynamic response, but they are easily affected by changes in the motor parameters. At present, the sensorless control methods such as the model reference adaptive system (MRAS), the extended Kalman filter (EKF) method and the observer estimation method have attracted much attention due to the superiority of the algorithm. The MRAS takes the mathematical model of the actual observation object as the reference model to establish the same adjustable model [15]. The method also gradually reduces the estimation error through the feedback link. However, it is assumed that the adjustable model and reference model have the same parameters, so it is necessary to combine the motor parameter on-line identification method to further improve its estimation accuracy. The EKF [16], [17] has high observation accuracy and strong robustness. However, the calculation process of this method is too complicated. Especially in the observation of high-speed PMSM, it is very difficult for the algorithm to complete the operation. Compared with the above methods, the SMO, an observer estimation method, is widely used in sensorless control strategy. Based on the theoretical basis of the sliding mode variable structure control, a special sliding mode control method is used to adjust the structure by altering the switching function so that the estimated value quickly approaches the real value [18]–[21]. The SMO has the characteristics of nonlinearity, high observation accuracy and strong robustness. However, the algorithm also has the disadvantage of the sliding mode variable structure being characterized by discontinuous Bang-Bang control, which can produce high-frequency chattering. In response to this problem, Chi [22] proposed a new SMO control strategy in which the saturation function is used. However, the introduction of a low-pass filter and additional position compensation of the rotor usually causes phase delay, and the control requirements of high performance applications cannot be met. Kim *et al.* [19] proposed a new SMO control strategy to reduce the estimated speed chattering of the motor, in which the switching function is replaced by a sigmoid function. Feng *et al.* [24] presented a four-level iterative SMO control strategy. A smaller value can be chosen as the sliding mode gain in the motor high-speed range, which can reduce the back-electromotive force (EMF) estimated error. The sliding mode gain is determined step by step on the basis of the selected test data to meet the Lyapunov stability condition. Feng proposed a high-order terminal non-singular SMO control strategy [25] in which the discrete output value of the traditional sliding mode switching function is integrated as the continuous sliding mode control input. It can not only reduce chattering but also eliminate the traditional SMO filter link. Although the low pass filter and phase compensation part are not used, the arc-tangent method is introduced to extract the rotor position according to the estimated orthogonal EMF components in these papers. However, in the process of calculating the rotor position using the arc-tangent method, the existence of noise and harmonics may influence the accuracy of the position estimation. Especially when the EMF crosses zero, obvious estimation error may occur due to the noise signals. In [26], a full-order SMO based on the effective back-EMF is proposed to estimate the rotor position and rotational speed of the PMSM. The observer can filter out the estimated high-frequency slip noise, which is contained in the effective back-EMF. However, the magnitude of the extended EMF is a function of rotor speed and stator current and a derivative of stator current, which means that the load condition will affect the magnitude of the extended EMF. In the shearer working process, the end drum load will cause significant distortions of the waveforms of the extended EMF components of a state transient.

In view of the above problems, this paper presents a shearer PMSRCTS, which consists of a low-speed large torque permanent magnet synchronous motor, three-stage reducer and

cutting drum. Because the motor output speed is low and the planetary gear reducer is eliminated, the system can effectively reduce the failure rate. A sensorless control strategy is designed for the system based on a new SMO. The phase-locked loop technique is used instead of the traditional arc-tangent function estimation, and the sigmoid function is introduced to replace the traditional sign function in the new SMO. The stable sliding mode gain is obtained by the Lyapunov stability condition and adjusted through the fuzzy adaptive control algorithm. To verify the validity and accuracy of the scheme, the mathematic model of the IPMSM and end cutting load changing are established. The results show that the proposed new SMO has good dynamic response, high observation accuracy and robustness. Sensorless control for the shearer PMSRCTS has a better control effect.

II. THE COMPOSITION OF THE PMSRCTS AND THE DESIGN OF THE SENSORLESS CONTROL STRATEGY

Shearer PMSRCTS is shown in Fig. 1. The mine explosion-proof, low-speed, high-torque PMSM is used as a driving source. It can generate large torque at low speeds. The motor output shaft is a hollow shaft with an internal spline, which connects to the gear shaft through an elongated, flexible torque shaft. The PMSM output torque is passed to the end-cutting drum after a three-stage reducer, which can perform cutting work.

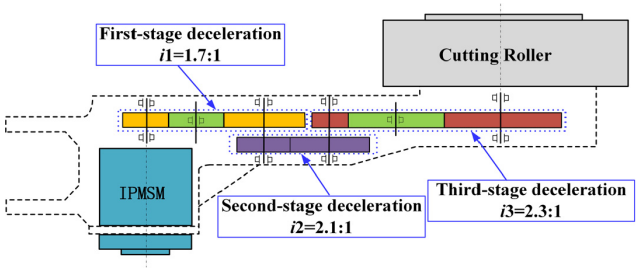

FIGURE 1. Schematic diagram of the PMSRCTS.

The sensorless control strategy for the shearer PMSRCTS is realized through DTC theory based on the new SMO. First, the shearer is started. Second, the traction system is started after the cutting drum speed reaches the command value. The drum is slowly cut into the coal seam. It is known that the coal block rate is related to the cutting thickness and that the cutting thickness is related to the cutting drum and the traction speed. Therefore, the drum speed command value can be calculated according to the required coal block rate and the feedback traction speed. The current value of the cutting motor or traction motor can be used as the feedback value for the traction speed adjustment, and the current can be obtained by the new SMO. Finally, the rotational speed and position information of the IPMSM rotor can be further obtained by observing the current value to realize sensorless control. However, the traction speed, the cutting drum speed and the coal-rock impedance are closely related to the load of the cutting drum, and the observation effect of SMO is directly affected by the load characteristics. Therefore, the influence of the load characteristics must be considered.

III. DESIGN AND OPTIMIZATION OF NEW SMO FOR IPMSM

The voltage mathematical model of the IPMSM in the synchronous rotating frame (d-q) is shown as follows:

$$\begin{pmatrix} u_d \\ u_q \end{pmatrix} = \begin{pmatrix} R + pL_d & -\omega_e L_q \\ \omega_e L_d & R + pL_q \end{pmatrix} \begin{pmatrix} i_d \\ i_q \end{pmatrix} + \begin{pmatrix} 0 \\ \omega_e \psi_f \end{pmatrix} \quad (1)$$

where u_d and u_q are the d and q axes of stator voltage. R is the stator resistance. i_d and i_q are the d and q axes of stator current. p is the differential operator, L_d and L_q are the d and q axes of inductances. ω_e is the rotor electrical speed, and ψ_f is the permanent magnet flux linkage.

According to the voltage mathematical model for the IPMSM in the synchronous rotation coordinate system, the dynamic system equation of the stator current is rewritten as follows,

$$\begin{pmatrix} \dot{i}_d \\ \dot{i}_q \end{pmatrix} = \begin{pmatrix} -\frac{R}{L_d} & \frac{\omega_e L_q}{L_d} \\ -\frac{\omega_e L_d}{L_q} & \frac{-R}{L_q} \end{pmatrix} \begin{pmatrix} i_d \\ i_q \end{pmatrix} + \begin{pmatrix} \frac{1}{L_d} & 0 \\ 0 & \frac{1}{L_q} \end{pmatrix} \begin{pmatrix} u_d - E_d \\ u_q - E_q \end{pmatrix} \quad (2)$$

where $E_d = 0$, $E_q = \omega_e \psi_f$, can be seen as the induced EMF in the d-q coordinates system.

A. THE DESIGN OF SMO AND STABILITY ANALYSIS

To obtain the value of the induced EMF in (2), SMO can be designed as [27]

$$\begin{pmatrix} \dot{\hat{i}}_d \\ \dot{\hat{i}}_q \end{pmatrix} = \begin{pmatrix} -\frac{R}{L_d} & \frac{\omega_e L_q}{L_d} \\ -\frac{\omega_e L_d}{L_q} & \frac{-R}{L_q} \end{pmatrix} \begin{pmatrix} \hat{i}_d \\ \hat{i}_q \end{pmatrix} + \begin{pmatrix} \frac{u_d - ksgn\left(\hat{i}_d - i_d\right)}{L_d} \\ \frac{u_q - ksgn\left(\hat{i}_q - i_q\right)}{L_q} \end{pmatrix} \quad (3)$$

where $\hat{i}_d$, $\hat{i}_q$ are the d and q axes of the stator observation current. k is the sliding mode gain. sgn is the sign function.

The state equation of the current error system can be obtained through the (2) and (3) subtraction as follows:

$$\begin{pmatrix} \dot{\tilde{i}}_d \\ \dot{\tilde{i}}_q \end{pmatrix} = \begin{pmatrix} -\frac{R}{L_d} & \frac{\omega_e L_q}{L_d} \\ -\frac{\omega_e L_d}{L_q} & \frac{-R}{L_q} \end{pmatrix} \begin{pmatrix} \tilde{i}_d \\ \tilde{i}_q \end{pmatrix} + \begin{pmatrix} \frac{E_d - ksgn\left(\hat{i}_d - i_d\right)}{L_d} \\ \frac{E_q - ksgn\left(\hat{i}_q - i_q\right)}{L_q} \end{pmatrix} \tag{4}$$

where $\tilde{i}_d = \hat{i}_d - i_d, \tilde{i}_q = \hat{i}_q - i_q$ are the current observation errors.

The current error observation (4) can be rewritten in vector form as follows,

$$\dot{\tilde{\boldsymbol{i}}} = \boldsymbol{A}\tilde{\boldsymbol{i}} + \boldsymbol{BE} + ksgn\left(\tilde{\boldsymbol{i}}\right) \tag{5}$$

where $\tilde{\boldsymbol{i}} = \begin{bmatrix} \tilde{i}_d & \tilde{i}_q \end{bmatrix}^T, \boldsymbol{E} = \begin{bmatrix} E_d & E_q \end{bmatrix}^T,$

$$\boldsymbol{A} = \begin{pmatrix} -\frac{R}{L_d} & \frac{L_q}{L_d}\omega_e \\ -\frac{L_d}{L_q}\omega_e & -\frac{R}{L_q} \end{pmatrix}, \quad \boldsymbol{B} = \begin{pmatrix} \frac{1}{L_d} & 0 \\ 0 & \frac{1}{L_q} \end{pmatrix}.$$

The SMO is used to estimate the current, and its sliding mode plane is defined as,

$$\boldsymbol{S} = \begin{bmatrix} \tilde{i}_d & \tilde{i}_q \end{bmatrix}^T = \boldsymbol{0} \tag{6}$$

According to the Lyapunov theorem, when the condition $\boldsymbol{S}^T\dot{\boldsymbol{S}} \leq \boldsymbol{0}$ is satisfied, the SMO enters the sliding mode and the error equation enters a steady state. When the sliding mode gain is large enough, the equivalent control can be defined as,

$$\boldsymbol{E_{eq}} = [\, ksgn\left(\hat{i}_d - i_d\right) \quad ksgn\left(\hat{i}_q - i_q\right) \,]^T \tag{7}$$

According to (7), the equivalent control amount can be defined as,

$$\boldsymbol{E_{eq}} = \begin{pmatrix} V_d \\ V_q \end{pmatrix} = \begin{pmatrix} \left[ksgn\left(\hat{i}_d - i_d\right)\right]_{eq} \\ \left[ksgn\left(\hat{i}_q - i_q\right)\right]_{eq} \end{pmatrix} = \begin{pmatrix} 0 \\ \omega_e\psi_f \end{pmatrix} \tag{8}$$

The expression of the sliding mode gain k can be calculated according to the sliding mode arrival condition $\boldsymbol{S}^T\dot{\boldsymbol{S}} \leq \boldsymbol{0}$

$$k \geq max \begin{pmatrix} \frac{E_d}{L_d} sgn\left(\tilde{i}_d\right) - \left(\frac{R}{L_d} + \frac{L_d}{L_q}\omega_e\right)\left|\tilde{i}_d\right|, \\ \frac{E_q}{L_q} sgn\left(\tilde{i}_q\right) - \left(\frac{R}{L_q} - \frac{L_q}{L_d}\omega_e\right)\left|\tilde{i}_q\right| \end{pmatrix} \tag{9}$$

B. ROTOR POSITION ESTIMATION BASED ON PLL

The purpose of SMO is to determine the estimated value of the d-q axis-induced EMF. It can be seen from (2) that the induced EMF of the q axis contains rotor speed information, $E_q = \omega_e\psi_f$. Thus, the estimated value of the q axis can be obtained according to (8), and the rotor speed can be obtained as follows,

$$\hat{\omega}_e = \frac{V_q}{\psi_f} \tag{10}$$

Although (10) can be used to obtain the position of the rotor angle, the motor in the process of cutting coal and rock, the permanent magnet flux chain is not a constant value due to the harsh working environment, the temperature and load change. There is some rotor position and speed error between the estimated and the actual value, which can affect the dynamic performance of the entire system.

For better dynamic performance, the PLL technology is used. It is an adaptive closed-loop system with excellent real-time tracking and estimation of the actual rotor position information; even in the voltage phase, angle imbalance, harmonics and other conditions also have better tracking performance. Since the winding of the motor is symmetrical, it is assumed that the motor terminal voltage of the three-phase stator winding [28] is as follows,

$$\begin{cases} u_a = u\cos\omega_e t \\ u_b = u\cos\left(\omega_e t - 2\pi/3\right) \\ u_c = u\cos\left(\omega_e t + 2\pi/3\right) \end{cases} \tag{11}$$

where u is the motor terminal voltage amplitude, $\theta_e = \omega_e t$, $\omega_e = \pi p_n n/30$, p_n is the motor pole pairs, and n is the mechanical speed of the motor rotor.

According to the transformation theory of synchronous rotation coordinates, the transformation matrix of the three-phase voltage transform to the d-q coordinate system [28] is

$$T\left(\hat{\theta}_e\right) = \frac{2}{3}\begin{pmatrix} cos\hat{\theta}_e & cos\left(\hat{\theta}_e - \frac{2}{3}\pi\right) & cos\left(\hat{\theta}_e + \frac{2}{3}\pi\right) \\ -sin\hat{\theta}_e & -sin\left(\hat{\theta}_e - \frac{2}{3}\pi\right) & -sin\left(\hat{\theta}_e + \frac{2}{3}\pi\right) \end{pmatrix} \tag{12}$$

where $\hat{\theta}_e$ is the estimated phase angle obtained using PLL technology, and $\hat{\theta}_e = \hat{\omega}_e t$.

$\tilde{\theta}_e = \hat{\theta}_e - \theta_e$ is the estimation error of the PLL. As long as the proper adjustment is made, the estimated value can be converted to the actual value of the rotor position.

When the neutral point isolation is considered, generally, it does not contain zero sequence components. Substituting the transformation matrix $T\left(\hat{\theta}_e\right)$ into (11),

$$\begin{pmatrix} V_d \\ V_q \end{pmatrix} = \begin{pmatrix} usin\left(\hat{\theta}_e - \theta_e\right) \\ ucos\left(\hat{\theta}_e - \theta_e\right) \end{pmatrix} \tag{13}$$

When the estimated value tracks the actual position of the rotor, the error is zero. According to the definition of the synchronous rotation d-q coordinate system, it can be defined as $V_{dref} = V_d = 0$

Therefore, a closed-loop PI regulator can be established according to (13). The rotor position information can be obtained. The specific block diagram is shown in Fig. 2.

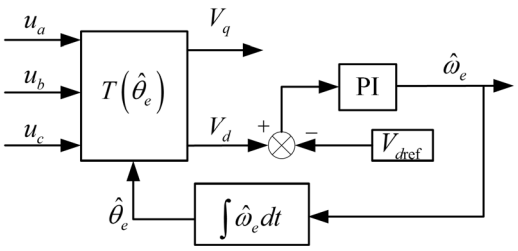

FIGURE 2. Block diagram of rotor position based on PI regulator.

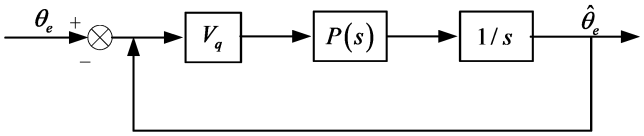

FIGURE 3. Closed-loop block diagram based on PI regulator.

According to (16), a closed-loop control block diagram can be obtained based on the PI regulator, as shown in Fig. 3.

The closed-loop transfer function of the system can be obtained from Fig. 3

$$G(s) = \frac{\hat{\theta}_e(s)}{\theta_e(s)} = \frac{V_q P(s)}{s + V_q P(s)} \tag{14}$$

In addition, the form of the PI regulator's transfer function is as follows,

$$P(s) = \gamma_p + \frac{\gamma_i}{s} \tag{15}$$

Upon substituting (15) into (14), the closed-loop transfer function becomes

$$G(s) = \frac{V_q\left(\gamma_p + \frac{\gamma_i}{s}\right)}{s + V_q\left(\gamma_p + \frac{\gamma_i}{s}\right)} = \frac{\sqrt{2}\omega_n s + \omega_n^2}{s^2 + \sqrt{2}\omega_n s + \omega_n^2} \tag{16}$$

According to the desired bandwidth of the closed-loop system, the PI regulator's parameters can be obtained

$$\gamma_p = \frac{\sqrt{2}\omega_n}{V_q}, \quad \gamma_i = \frac{\omega_n^2}{V_q} \tag{17}$$

C. OPTIMIZATION OF FUZZY SLIDING MODE OBSERVER BASED ON NEW SWITCHING FUNCTION

Because the ideal switching function is used in the above SMO, the discontinuous open-loop characteristic can result in a large chattering for the observer's value during the switching process. At the same time, in order to increase the anti-interference ability of the observer and ensure the generation of sliding mode, the sliding mode switching gain is usually chosen to be too large, but this will further increase the chattering noise in the state estimate. Therefore, it is possible to reduce the chattering noise in the system by improving the ideal switching function and introducing the intelligent control method to effectively estimate the switching gain according to the sliding mode arrival condition.

First, the ideal switching function is improved in the designed SMO. Then, the fuzzy rule is designed according to the fuzzy control theory for optimizing the switching gain. Finally, the switchover gain is effectively estimated according to the sliding mode arrival condition. The new sigmoid function is as follows,

$$sigmoid(s) = \frac{2}{1 + e^{-as}} - 1 \tag{18}$$

where a is a tunable parameter, $a = 3$. When a takes different values, the boundary layer function curve is different. The larger the value of a is, the higher is the boundary layer changing rate. The curve becomes steep and is close to the ideal switching function. Since the sigmoid function has a continuous switching characteristic, it can effectively suppress chattering. The SMO can be written as,

$$\begin{pmatrix} \dot{\hat{i}}_d \\ \dot{\hat{i}}_q \end{pmatrix} = \begin{pmatrix} -\frac{R}{L_d} & \frac{\omega_e L_q}{L_d} \\ -\frac{\omega_e L_d}{L_q} & \frac{-R}{L_q} \end{pmatrix} \begin{pmatrix} \hat{i}_d \\ \hat{i}_q \end{pmatrix} + \begin{pmatrix} \frac{u_d - ksigmoid\left(\hat{i}_d - i_d\right)}{L_d} \\ \frac{u_q - ksigmoid\left(\hat{i}_q - i_q\right)}{L_q} \end{pmatrix} \tag{19}$$

When the system is in sliding mode motion, if the absolute value of the error $|S|$ between the actual value and the estimated value is large, the system is far from the sliding surface, and when it is small, the system approaches the sliding surface. If S is a positive larger value, the control system should enter a larger control signal in the positive direction so that the system can move to the sliding surface. Similarly, if S is a larger negative value, the control system should enter a larger control signal in the negative direction. The direction of the system input can be achieved by the above sigmoid function, and the size of the control depends on the size of the sliding mode gain. Therefore, according to the size of the error S, the sliding mode switch gain can be optimized through the fuzzy control strategy. Combining the fuzzy control theory, the error S can be chosen as the input of the fuzzy controller, where Ks is the output. The output of the fuzzy controller is the proportional factor of the sliding mode switching gain. The input and output of the fuzzy controller are quantized so that the input interval is $[-3, 3]$ and the output interval is $[0, 3]$.The fuzzy language variables are defined for input and output, where the fuzzy language of the input variable is {NB(Negative Big), NM(Negative Middle), NS(negative small), ZR(zero), PS(positive small), PM(positive middle), PB(positive big)}, the output variable is { ZR(zero), PS(positive small), PM(positive middle), PB(positive big)}.

Through the above analysis, the input field of the fuzzy controller is defined as seven fuzzy subsets. Four fuzzy subsets are defined on the output domain. The trigonometric function is used to design the membership function of the input and output, and the degrees of membership for the input and output are shown as Figs. 4 and 5.

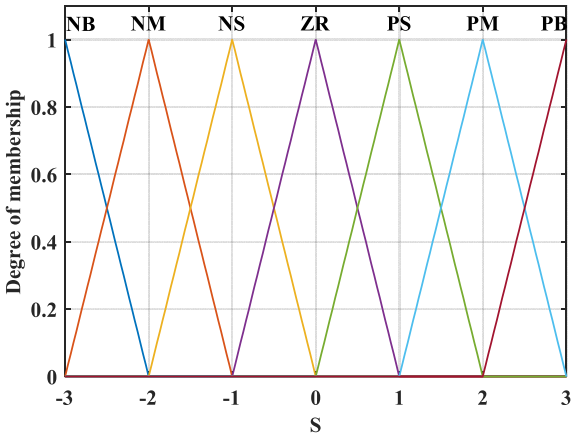

FIGURE 4. Fuzzy input membership functions.

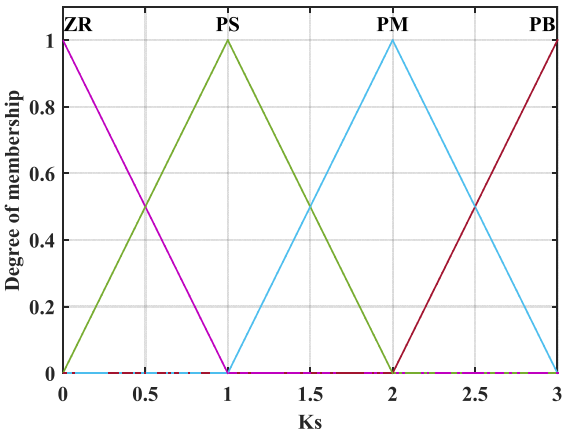

FIGURE 5. Fuzzy output membership functions.

Based on the Mamdani type fuzzy logic reasoning, the rules are as follows,

Rule 1: If the input error S is NB, then the output proportional factor Ks is PB;

Rule 2: If the input error S is NM, then the output proportional factor Ks is PM;

Rule 3: If the input error S is NS, then the output proportional factor Ks is PS;

Rule 4: If the input error S is ZR, then the output proportional factor Ks is ZR;

Rule 5: If the input error S is PS, then the output proportional factor Ks is PS;

Rule 6: If the input error S is PM, then the output proportional factor Ks is PM;

Rule 7: If the input error S is PB, then the output proportional factor Ks is PB;

Finally, the fuzzy outputs need to be converted to precise variables through centroid defuzzification method. The switching gain can be adjusted through the output proportional factor of the sliding mode switch. The chattering reduced structure of the observer is shown as Fig. 6,

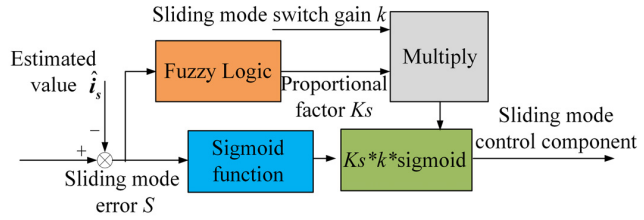

FIGURE 6. Chattering reduced structure of the observer.

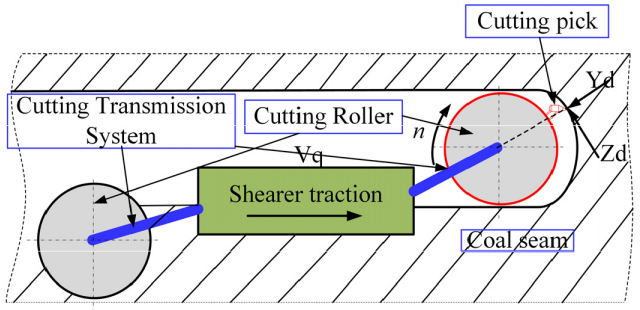

FIGURE 7. Shearer cutting process diagram.

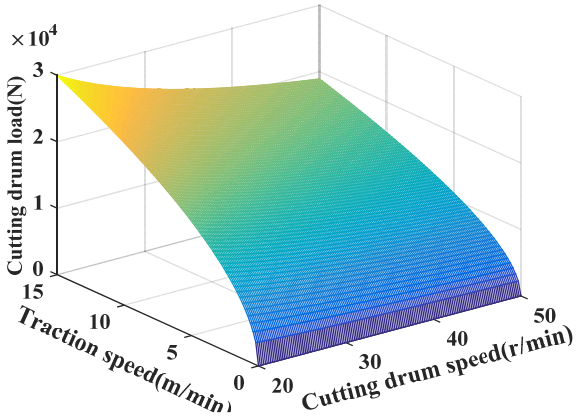

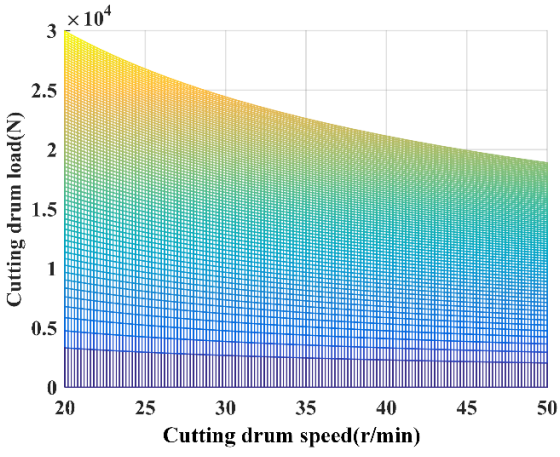

FIGURE 8. The relationship among cutting load torque, traction speed and drum cutting speed.

IV. THE MATHEMATICAL MODEL OF SHEARER CUTTING DRUM LOAD

The change of the shearer cutting load characteristics has a great influence on the sensorless control strategy of

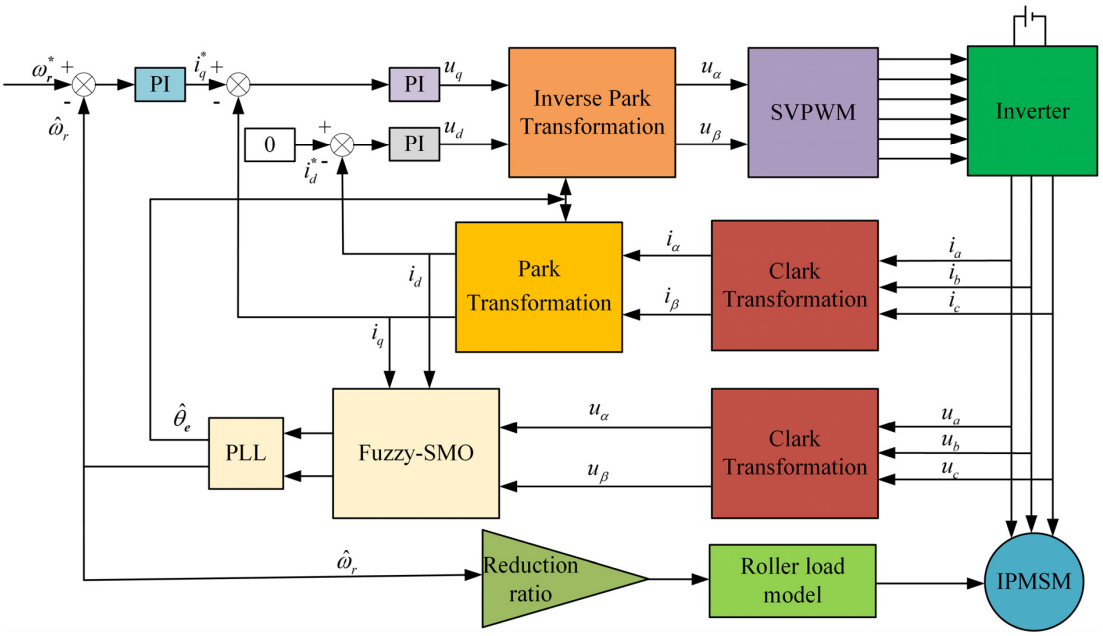

FIGURE 9. Sliding mode control block diagram.

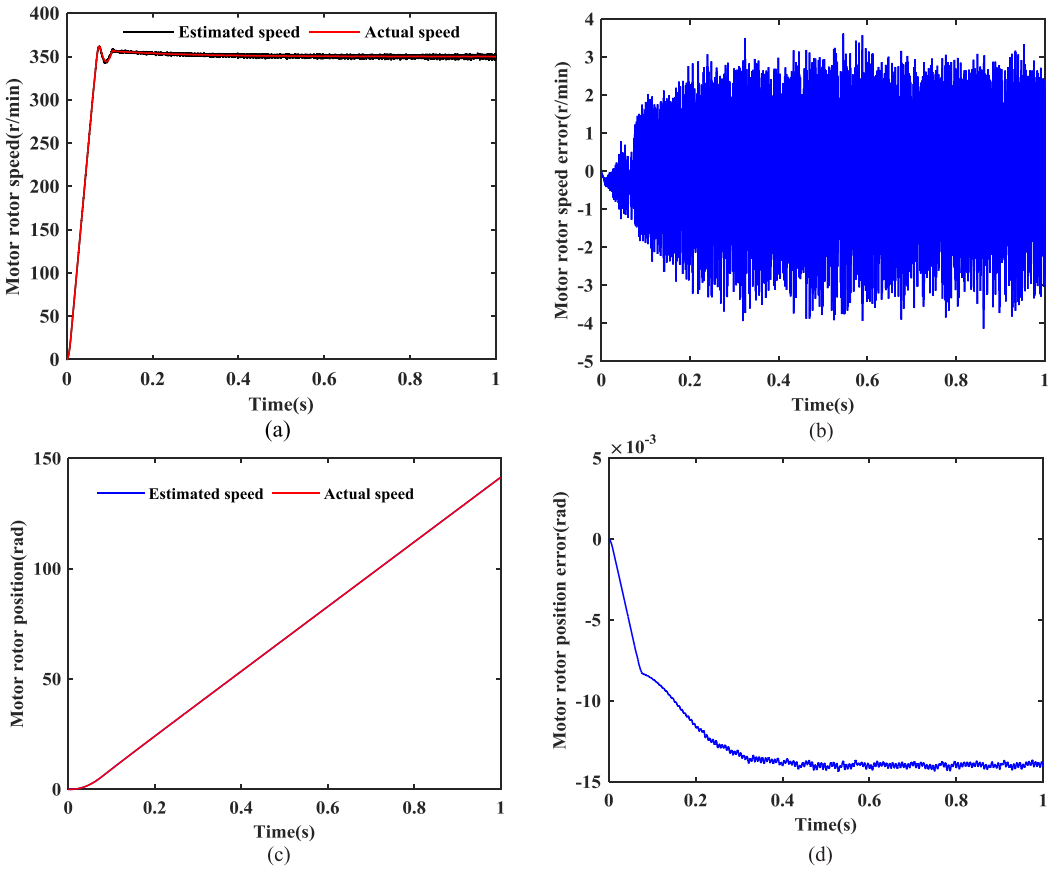

FIGURE 10. Simulation results obtained by the proposed SMO using sign function: (a) The speed of the IPMSM rotor. (b) Estimated motor speed error. (c) The position of the IPMSM rotor. (d) Estimated motor position error.

the IPMSM. The change in load directly affects the observation effect of the new SMO, so it is necessary to establish the mathematical model of the shearer cutting load. In the continuous cutting process, the spiral drum not only rotates around the drum axis but also continues at a certain traction speed. During the rotation of the drum for one circle, each

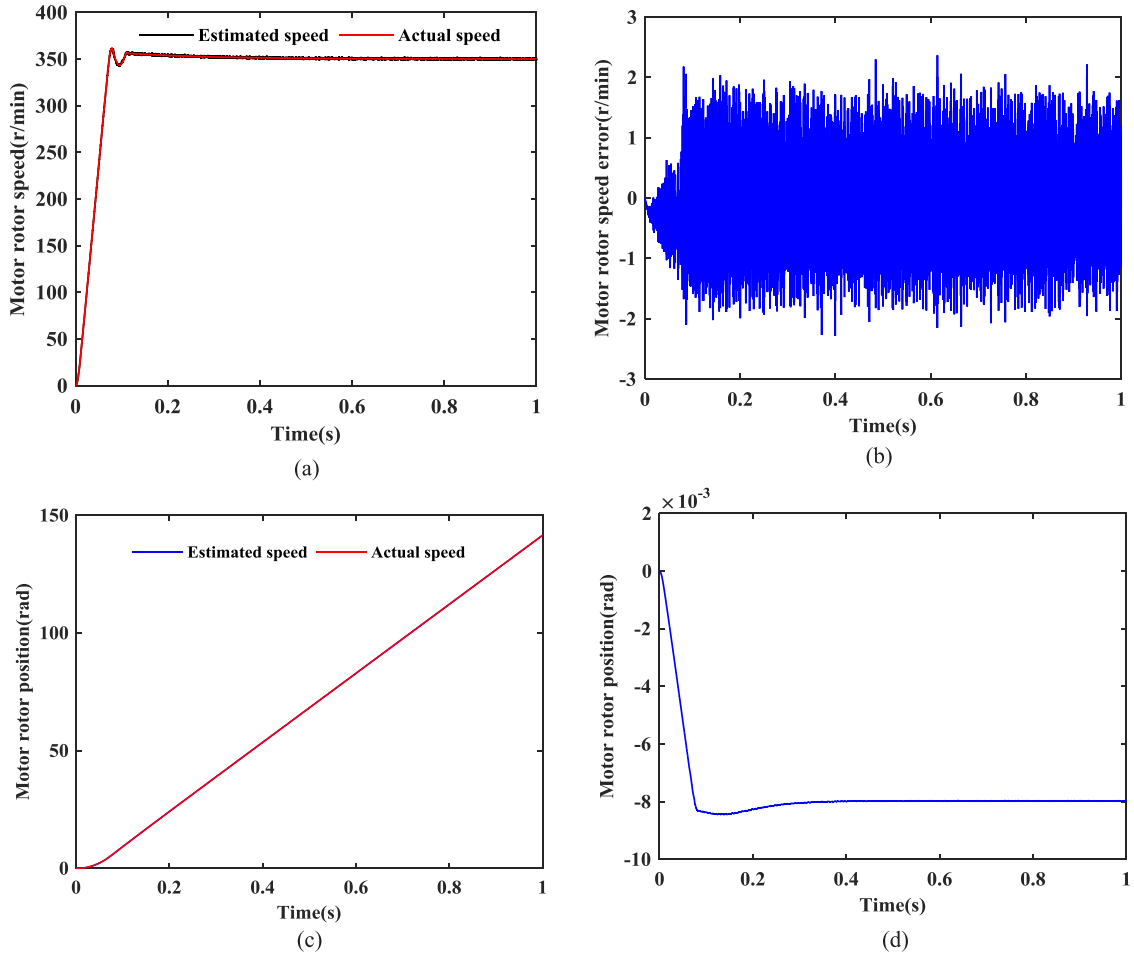

FIGURE 11. Simulation results obtained by the proposed SMO using sigmoid function and fuzzy logic: (a) The speed of the IPMSM rotor. (b) Estimated motor speed error. (c) The position of the IPMSM rotor. (d) Estimated motor position error.

pick is only half the time in the cutting coal and rock. The shearer cutting process is shown in Fig. 7.

The cutting thickness is related to the traction speed, the cutting drum speed and the pick configuration. The maximum cutting thickness [29] is,

$$h_{max} = \frac{100V_q}{mn} \tag{20}$$

The average cutting thickness is,

$$\bar{h} = \frac{2}{\pi} h_{max} \tag{21}$$

where V_q is the traction speed of the shearer, m/min. n is the cutting drum speed, r/min. m is the number of cutting picks on the i-th cutting line, which depends on the pick configuration and the number of spiral blades.

To study the cutting transmission system and traction system of the shearer, the cutting resistance and traction resistance model of the cutting drum are established. The drum load is closely related to the coal and rock parameters, props shape, pick arrangement, and machine movement. Generally, the drum load is calculated by the former Soviet Union method [29], [30]. The average cutting force Z_d on a single blunt pick is,

$$Z_d = Z_0 + f'(Y_d - Y_0) \tag{22}$$

where Z_0 is the average cutting force on a single sharp pick. $Y_d - Y_0$ is the increased part when the cutting picks are blunt, and $Y_d - Y_0 = 100\delta_{cm} S_a K_\delta$, δ_{cm} is the uniaxial compressive strength of coal; according to experience, $\delta_{cm} = 10f$, $10 \sim 50$ MPa. f is the rock strength coefficient. When the coal seam is soft coal, $f \leq 1.5$. When the coal seam is hard, $f = 1.5 \sim 20$. S_a is the projected area of the wear surface on the cutting plane. When the cutter is a pick, $S_a = 0.15 \sim 0.2$ cm^2. K_δ is the ore body stress state volume coefficient. The range is 0.8∼1.59. The higher the brittleness is, the smaller is the value. f' is the anti-cutting resistance coefficient. The range is 0.38∼0.42. The maximum value should be taken for the large cutting thickness.

The average cutting force on a single sharp pick is,

$$Z_0 = \frac{10A_P\left(0.35b_p + 0.3\right)\bar{h}l_i K_Z K_Y K_\varphi K_C K_{ot}}{\left(b_p + K_\psi \bar{h}^{0.5}\right)cos\beta} \tag{23}$$

where A_p is the coal average cutting impedance, $A_p = 130f$. b_p is the calculation width of the pick

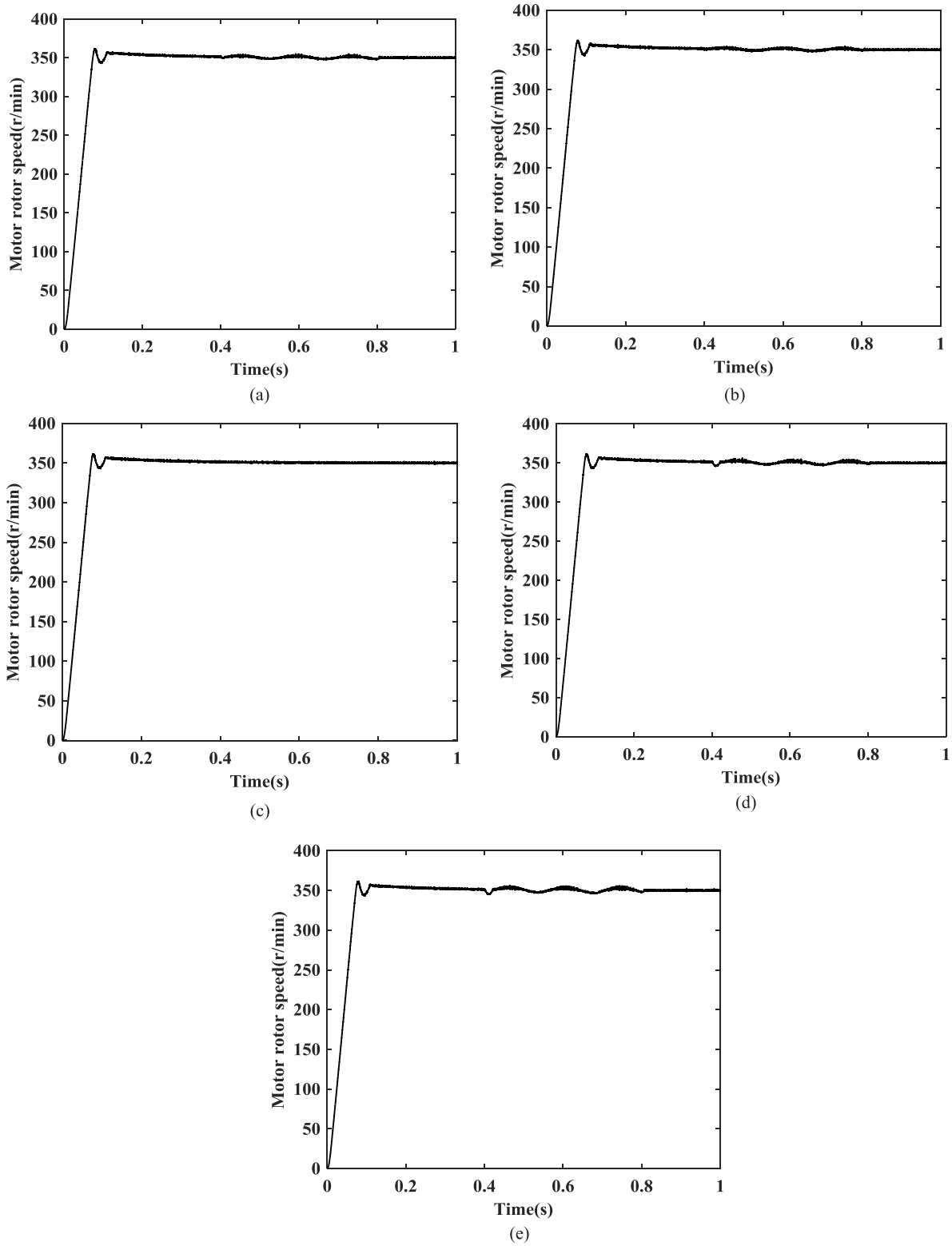

FIGURE 12. Estimated speed curves obtained by the proposed SMO using sigmoid function and fuzzy logic when motor parameters changed: (a) Only stator resistance R changed. (b) Only d axis inductance L_d changed. (c) Only q axis inductance L_q changed. (d) Only permanent magnet flux linkage ψ_f changed. (e) All motor parameters R, L_d, L_q and ψ_f changed.

working part. K_z is the free expression factor. K_Y is the influence coefficient of the cutting angle α. The range is 0.9∼1.34. K_φ is the shape influence coefficient of the cutting pick rake face. The range is 0.85∼0.9. K_c is the cutting pick arrangement coefficient. When the cutting pick is the sequential arrangement, $K_c = 1$. When the cutting

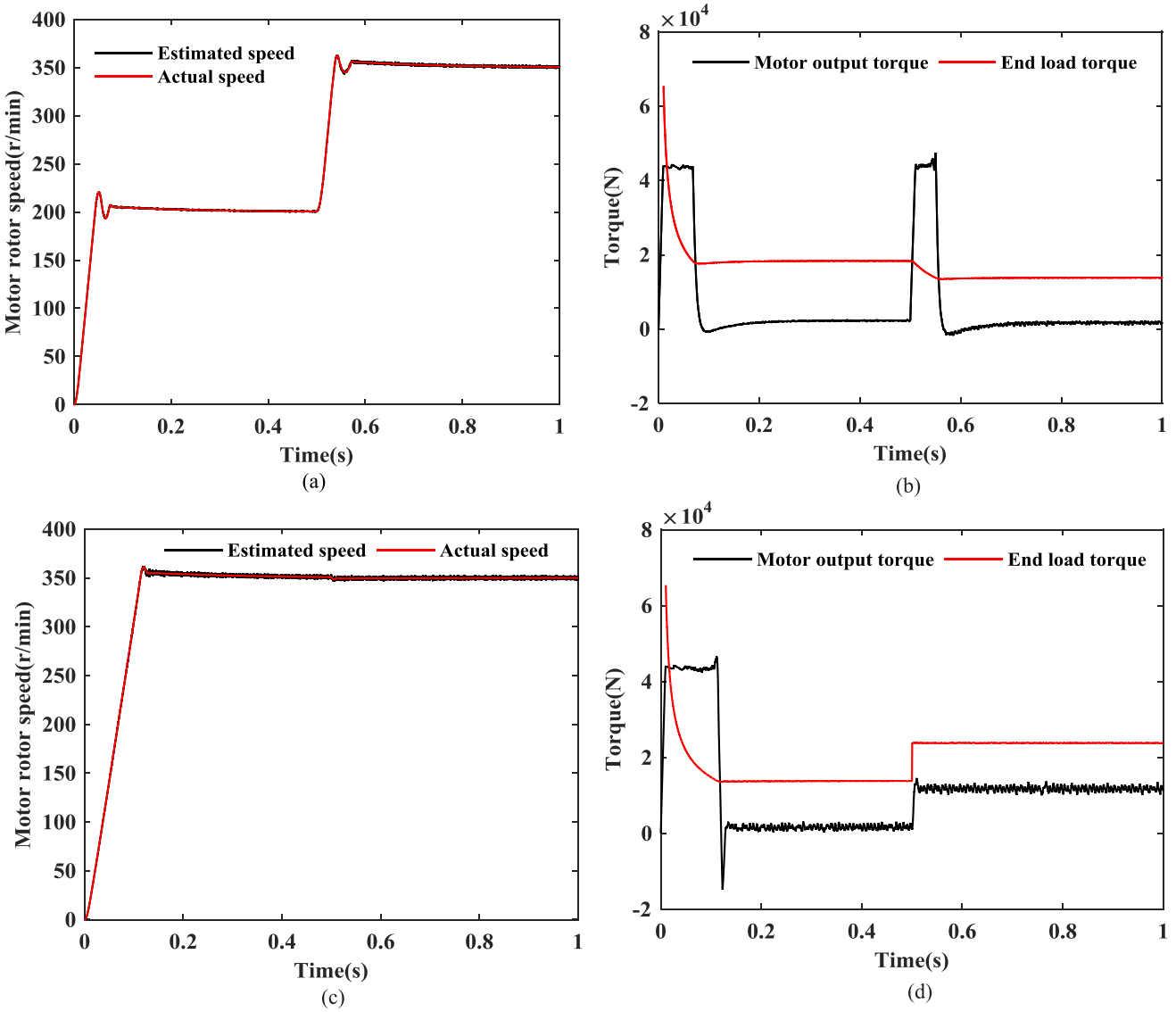

FIGURE 13. The speed and torque: (a) The speed of the IPMSM when the reference speed changed. (b) The output torque of the IPMSM and the end load torque when the reference speed changed. (c) The speed of the IPMSM when the end load torque changed. (d) The output torque of the IPMSM and the end load torque when the end load torque changed.

pick is the checkerboard arrangement, $K_c = 1.25$. K_{ot} is influence coefficient of ground pressure on coal face in working face. K_ψ is coal brittleness coefficient. The range is 2.1∼3.5. β is the deflection angle of the picks relative to the traction direction for a cutting line. The average drum load torque is,

$$M_Z = 0.5D\sum\left(\frac{10A_P\left(0.35b_p+0.3\right)\bar{h}l_iK_ZK_YK_\varphi K_CK_{ot}}{\left(b_p+K_\psi\bar{h}^{0.5}\right)cos\beta} + 100f'\delta_{cm}S_aK_\delta\right) \tag{24}$$

where D is the drum diameter, D=200 cm.

It can be seen from the (22) that the mathematical model of the cutting drum load is a binary function whose independent variable is the shearer drum speed and the traction speed. The relationship is shown in Fig. 8.

V. NUMERICAL SIMULATIONS AND ANALYSIS

To verify the observed effect, the robustness of the new SMO and the validity of the sensorless control strategy, the discrete model is used to build the simulation model, which must be discretized for the continuous time system. The inverse differential transformation method is used to discretize the current observation equation.

$$\begin{cases}\hat{i}_d(k+1) = A_d\hat{i}_d(k) + B_d\left[u_d(k) - V_d(k) + \omega_eL_q\hat{i}_q(k)\right]\\ \hat{i}_q(k+1) = A_q\hat{i}_q(k) + B_q\left[u_q(k) - V_q(k) + \omega_eL_d\hat{i}_d(k)\right]\end{cases} \tag{25}$$

where $A_d = exp\left(-R/L_dT_s\right), B_d = \frac{1}{R}\left(1-A_d\right), A_q = exp\left(-R/L_qT_s\right), B_q = \frac{1}{R}\left(1-A_q\right)$.

The system shown in Fig. 9 has been implemented in the Matlab/Simulink programming environment, and the IPMSM

TABLE 1. Simulation parameters of IPMSM.

parameters	Value
Rated power（kW）	300
Rated voltage（V）	1140
Pole pairs number	4
Stator resistance（mΩ）	25
Flux linkage（Wb）	3.56
D-axis inductance (H)	0.021
Q-axis inductance (H)	0.0032

parameters are listed in Table 1. As seen from the fourth part, the shearer cutting load is directly related to the drum speed and traction speed. To study the control effect of the sensorless control strategy, the traction speed is set to the rated value, $V_q = 2$ m/min, and the reference speed of the IPMSM is set to 350 r/min. The reduction ratio size is set to $i_z = 7.8$.

In the control of speed and current references, PI control is used to effectively reduce the accumulative errors and using the estimated position and speed of the rotor, the closed sensorless control of the motor is implemented. The PI parameters of the speed loop are the proportional gain $K_{sp} = 300$ and the integral gain $K_{si} = 1600$. The PI parameter of the d-axis and q-axis current loop are the proportional gain $K_{dp} = 42$, $K_{qp} = 6.4$ and integral gain $K_{di} = 50$, $K_{qi} = 50$, respectively. The sliding mode gain of SMO is $k = 1000$. The PI parameters of PLL are the proportional gain $K_{pp} = 60$ and integral gain $K_{pi} = 800$.

Fig. 10 shows the speed and position of the IPMSM rotor using a sign function. Fig. 11 shows the speed and position of the IPMSM rotor using a sigmoid function and fuzzy logic. In the simulation, the reference speed is changed from 0 to 350 r/min. It can be seen from Figs. 10 and 11 that the IPMSM rotor speed and position can be estimated from the proposed SMO and chattering phenomenon is reduced when the sign function is replaced by a sigmoid function with the fuzzy logic introduction. The robustness of the new SMO is studied by changing the internal parameters of the motor. Fig. 12 shows the estimated speed results when the IPMSM parameters used in the SMO have been changed. Fig. 12 (a) displays the result when the stator resistance R increases from 25 mΩ to 30 mΩ at 0.4 s and then decreases from 30 mΩ to the initial value 25 mΩ at 0.8 s. Fig. 12 (b) shows the speed change curve when L_d is changed from 21 mH to 26 mH at 0.4 s and then to the initial value of 21 mH at 0.8 s. Fig. 12(c) displays the result when L_q increased from 3.2 mH to 4.2 mH at 0.4 s and then decreased to the initial value of 4.2 mH at 0.8 s. Fig. 12 (d) gives the waveform when the ψ_f changes from 3.56 Wb to 3.36 Wb at 0.4 s and then increases to 3.56 Wb at 0.8 s. In Fig. 12(e), all parameters R, L_d, L_q and ψ_f are changed at the same time and parameters setting values are the same as in Fig. 12(a)-(d). As seen from Fig. 12, the estimated speed can still converge to the actual value when the motor parameters change, which verifies the robustness of the proposed program.

Fig. 13 (a) gives the result when the reference speed changed from 100 r/min to 350 r/min at 0.5 s. Fig. 13 (b) shows the end load torque and IPMSM output torque when reference speed changed from 100 r/min to 350 r/min at 0.5 s. Fig. 13 (c) displays the result when the end load torque increased 10000 N suddenly at 0.5 s. Fig. 13 (d) shows the end load torque and IPMSM output torque when Fig. 13 (c) displays the result when the end load torque increased 10000 N suddenly at 0.5 s. It can be seen from Fig. 13 that when the motor speed and end load change, the estimated speed can converge to the actual value quickly, which verifies the dynamic response capability of the proposed approach.

VI. CONCLUSIONS

This paper presents a PMSRCTS with low-speed and high-torque IPMSM as the driving source and sensorless control strategy for the PMSRCTS based on a new SMO. Because the motor output speed is low and the planetary gear reducer is eliminated, the system can effectively reduce the failure rate. In the new SMO, the phase locked loop technique is used instead of the traditional arc-tangent function estimation, and the sigmoid function is introduced to replace the traditional sign function. The stable sliding mode gain is obtained by the Lyapunov stability condition and adjusted through the fuzzy adaptive control algorithm. The dynamic response capability of the SMO is tested through speed changing and end load mutation. The robustness of the SMO is discovered by changing the internal parameters of the IPMSM. The results show that the proposed new SMO has good dynamic response capability, high observation accuracy and robustness.

REFERENCES

[1] N. Bilgin, M. A. Demircin, H. Copur, C. Balci, H. Tuncdemir, and N. Akcin, "Dominant rock properties affecting the performance of conical picks and the comparison of some experimental and theoretical results," *Int. J. Rock Mech. Mining Sci.*, vol. 43, no. 1, pp. 139–156, Jan. 2006.

[2] K. Oraee, N. Oraee , A. Goodarzi, and P. Khajehpour, "Effect of discontinuities characteristics on coal mine stability and sustainability: A rock fall prediction approach,"İ *Int. J. Mining Sci. Tech.*, vol. 26, no. 1, pp. 65–70, 2016.

[3] J. Zuo, Z. Wang, H. Zhou, J. Pei, and J. Liu, "Failure behavior of a rock-coal-rock combined body with a weak coal interlayer," *Int. J. Mining Sci. Tech.*, vol. 23, no. 6, pp. 907–912, 2013.

[4] G. W. Li, "Dynamic characteristics analysis of shearer electro-hydraulic short-range cutting transmission system under dynamic excitation," M.S. thesis, School Mech. Eng., Chongqing Univ., Chongqing, China, 2016.

[5] L. J. Zhao and Z. G. Sun, "Reliability study of thin seam hearer cutting unit under multi-condition," *Adv. Mater. Res.*, vols. 199–200, pp. 591–596, Apr. 2011.

[6] L.-J. Zhao and L.-W. Ma, "Thin seam shearer reliability analysis and fatigue life prediction," *J. China Coal Soc.*, vol. 38, no. 7, pp. 1287–1292, 2013.

[7] L.-J. Zhao and Y.-Z. Ma, "Reliability research on shearer cutting unit based on multi-body dynamics," *J. China Coal Soc.*, vol. 34, no. 9, pp. 1272–1275, 2009.

[8] L. Si, Z. Wang, X. Liu, C. Tan, and L. Zhang, "Cutting state diagnosis for shearer through the vibration of rocker transmission part with an improved probabilistic neural network," *Sensors*, vol. 16, no. 4, p. 479, Apr. 2016.

[9] Z. Li and Z. Peng, "Nonlinear dynamic response of a multi-degree of freedom gear system dynamic model coupled with tooth surface characters: A case study on coal cutters," *Nonlinear Dyn.*, vol. 84, no. 1, pp. 271–286, Apr. 2016.

[10] Y. Yang, J. H. Zou, D. T. Qin, and A. H. Yuan, "High reliability electromechanical-hydraulic short-range cutting transmission system of shearer," *J. Mech. Eng.*, vol. 52, no. 4, pp. 111–119, 2016.
[11] Y. L. Cheng, Z. M. Xiao, L. R. Huan, and F. Chen, "Simulation analysis of planetary gears train of semi-direct drive wind turbine based on Adams," *Appl. Mech. Mater.*, vols. 789–790, pp. 311–315, Sep. 2015.
[12] D. Paulus, J.-F. Stumper, and R. Kennel, "Sensorless control of synchronous machines based on direct speed and position estimation in polar stator-current coordinates," *IEEE Trans. Power Electron.*, vol. 28, no. 5, pp. 2503–2513, May 2013.
[13] K. Lu, X. Lei, and F. Blaabjerg, "Artificial inductance concept to compensate nonlinear inductance effects in the back EMF-based sensorless control method for PMSM," *IEEE Trans. Energy Convers.*, vol. 28, no. 3, pp. 593–600, Sep. 2013.
[14] Z. Xu and M. F. Rahman, "An adaptive sliding stator flux observer for a direct-torque-controlled IPM synchronous motor drive," *IEEE Trans. Ind. Electron.*, vol. 54, no. 5, pp. 2398–2406, Oct. 2007.
[15] D. P. Marcetic, I. R. Krcmar, M. A. Gecic, and P. R. Matic, "Discrete rotor flux and speed estimators for high-speed shaft-sensorless IM drives," *IEEE Trans. Ind. Electron.*, vol. 61, no. 6, pp. 3099–3108, Jun. 2014.
[16] Z. Xu and M. F. Rahman, "Comparison of a sliding observer and a Kalman filter for direct-torque-controlled IPM synchronous motor drives," *IEEE Trans. Ind. Electron.*, vol. 59, no. 11, pp. 4179–4188, Nov. 2012.
[17] D. Xu, S. Zhang, and J. Liu, "Very-low speed control of PMSM based on EKF estimation with closed loop optimized parameters," *ISA Trans.*, vol. 52, no. 6, pp. 835–843, Nov. 2013.
[18] Y. Zhao, W. Qiao, and L. Wu, "An adaptive quasi-sliding-mode rotor position observer-based sensorless control for interior permanent magnet synchronous machines," *IEEE Trans. Power Electron.*, vol. 28, no. 12, pp. 5618–5629, Dec. 2013.
[19] H. Kim, J. Son, and J. Lee, "A high-speed sliding-mode observer for the sensorless speed control of a PMSM," *IEEE Trans. Ind. Electron.*, vol. 58, no. 9, pp. 4069–4077, Sep. 2011.
[20] Z. Qiao, T. Shi, Y. Wang, Y. Yan, C. Xia, and X. He, "New sliding-mode observer for position sensorless control of permanent-magnet synchronous motor," *IEEE Trans. Ind. Electron.*, vol. 60, no. 2, pp. 710–719, Feb. 2012.
[21] G. Wang, Z. Li, G. Zhang, Y. Yu, and D. Xu, "Quadrature PLL-based high-order sliding-mode observer for IPMSM sensorless control with online MTPA control strategy," *IEEE Trans. Energy Convers.*, vol. 28, no. 1, pp. 214–224, Mar. 2013.
[22] S. Chi, Z. Zhang, and L. Xu, "Sliding-mode sensorless control of direct-drive PM synchronous motors for washing machine applications," *IEEE Trans. Ind. Appl.*, vol. 45, no. 2, pp. 582–590, Mar. 2009.
[23] H. Lee and J. Lee, "Design of iterative sliding mode observer for sensorless PMSM control," *IEEE Trans. Control Syst. Technol.*, vol. 21, no. 4, pp. 1394–1399, Jul. 2013.
[24] Y. Feng, J. Zheng, X. Yu, and N. V. Truong, "Hybrid terminal sliding-mode observer design method for a permanent-magnet synchronous motor control system," *IEEE Trans. Ind. Electron.*, vol. 56, no. 9, pp. 3424–3431, Sep. 2009.
[25] L. Guo, Z. Xing, S. Yang, and R. Cao, "Speed sensorless control for salient permanent magnet synchronous wind generators," *Autom. Electr. Power Syst.*, vol. 38, no. 22, pp. 108–112 and 122, 2014.
[26] H.-X. Wang, F. Xiao, W.-M. Ma, M.-L. Chen, and Y. Liu, "Sensorless control of PMSG based on sliding mode observer and software phase locked-loop," *Electr. Mach. Control*, vol. 15, no. 1, pp. 49–54, 2011.
[27] C. X. Li, *Shearer*. Beijing, China: China Coal Industry Publishing House, 1998.
[28] L. Yuan, B. X. Hu, K. Y. Wei, and S. Che, *Modern Permanent Magnet Synchronous Motor Control Principle and MATLAB Simulation*. Beijing, China: Beijing Univ. of Aeronautics and Astronautics Press, 2016.
[29] I. Evans, "Lateral spacing of point-attack picks," *Int. J. Rock Mech. Mining*, vol. 22, no. 2, pp. 7–10, 1984.
[30] I. Evans, "A theory of the cutting force for point-attack picks," *Int. J. Mining Eng.*, vol. 2, no. 1, pp. 63–71, Apr. 1984.

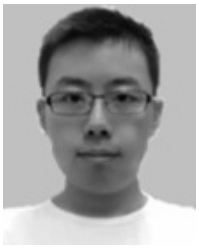

LIANCHAO SHENG was born in 1990. He received the B.E. and M.E. degrees from the School of Mechatronic Engineering, China University of Mining and Technology, Xuzhou, China, in 2014 and 2016, respectively, where he is currently pursuing the Ph.D. degree in the School of Mechatronic Engineering. His research interests include dynamic analysis and control of shearer cutter.

WEI LI was born in 1964. He received the B.E. degree from the School of Automation Engineer, University of Electronic Science and Technology of China, Chengdu, China, in 1986, and the M.E. and Ph.D. degrees from the China University of Mining and Technology, Xuzhou, China, in 1989 and 2004, respectively. From 1989 to 2004, he was to a Lecturer and the was promoted to an Associate Professor in the School of Mechatronic Engineering, China University of Mining and Technology, where he was a Professor in 2005 and has been the Dean since 2011. His research interests include structure design of shearer, mobile target collaboration positioning, metro stray current monitoring, optical fiber sensing, and network architecture.

YUQIAO WANG was born in 1974. He received the B.E., M.E., and Ph.D. degrees from the School of Mechatronic Engineering, China University of Mining and Technology, Xuzhou, China, in 1997, 2005, and 2012, respectively. He is currently with the China University of Mining and Technology as an Associate Professor. His current research interests include shearer dynamics, intelligent control of electro-mechanical system and design, and application of micro-electromechanical system.

MENGBAO FAN was born in 1981. He received the M.E. and Ph.D. degrees in control science and engineering from Zhejiang University, Hangzhou, China, in 2006, and 2009, respectively. He is currently with the China University of Mining and Technology as an Associate Professor. His current research interests include shearer dynamics, intelligent control of electro-mechanical system, and electromagnetic nondestructive testing theory.

XUEFENG YANG was born in 1979. He received the B.E., M.E., and Ph.D. degrees from the School of Mechatronic Engineering, China University of Mining and Technology, Xuzhou, China, in 2004, 2006, and 2009, respectively. He is currently with the China University of Mining and Technology as an Associate Professor. His current research interests include shearer dynamics, robot dynamics, intelligent detection and information processing, and design and application of micro-electromechanical system.